

## Impact of high spins on the ejection of mass in GW170817

E.R. MOST,<sup>1</sup> L.J. PAPENFORT,<sup>1</sup> A. TSOKAROS,<sup>2</sup> AND L. REZZOLLA<sup>1</sup>

<sup>1</sup>*Institut für Theoretische Physik, Goethe Universität Frankfurt am Main, Germany*

<sup>2</sup>*Department of Physics, University of Illinois at Urbana-Champaign, Urbana, IL 61801, US*

### ABSTRACT

Following the detection of GW170817 and the accompanying kilonova AT2017gfo, it has become crucial to model and understand the various channels through which mass is ejected in neutron-star binary mergers. We discuss the impact that high stellar spins prior to merger have on the ejection of mass focussing, in particular, on the dynamically ejected mass by performing general-relativistic magnetohydrodynamic simulations employing finite-temperature equations of state and neutrino-cooling effects. Using eight different models with dimensionless spins ranging from  $\chi \simeq -0.14$  to  $\chi \simeq 0.29$  we discuss how the presence of different spins affects the angular distribution and composition of the ejected matter. Most importantly, we find that the dynamical component of the ejected mass can be strongly suppressed in the case of high spins aligned with the orbital angular momentum. In this case, in fact, the merger remnant has an excess angular momentum yielding a more extended and “colder” object, with reduced ability to shed mass dynamically. We discuss how this result impacts the analysis of the recent merger event GW170817 and its kilonova afterglow.

*Keywords:* gravitational waves — gamma-ray burst: general — stars: neutron

### 1. INTRODUCTION

Following the detection of GW170817 (The LIGO Scientific Collaboration & The Virgo Collaboration 2017) and the subsequent electromagnetic counterpart (LIGO Scientific Collaboration et al. 2017), it has been possible to extract a number of different constraints and conclusions on the equation of state (EOS) of nuclear matter. Among them are the constraints on the maximum mass of isolated neutron nonrotating (Margalit & Metzger 2017; Shibata et al. 2017; Rezzolla et al. 2018; Ruiz et al. 2018) and on the possible ranges for radii of neutron stars (Annala et al. 2018; Most et al. 2018; Tews et al. 2018; Burgio et al. 2018; Raithel et al. 2018). In addition to the gravitational-wave signal, a crucial input for some of these works is the ejected mass from the merger site that has undergone nucleosynthesis and is hence responsible for the observed kilonova light curves (Kasen et al. 2017; Drout et al. 2017). Hence, having a very accurate modelling of the mass ejection and its origins is of great importance and several studies have already been made to elucidate the ejection mechanism

and quantify the various ejection channels. Numerical simulations classify the ejection in terms of matter that is *dynamically* ejected (Hotokezaka et al. 2013; Bauswein et al. 2013; Radice et al. 2016, 2018; Palenzuela et al. 2015; Lehner et al. 2016; Sekiguchi et al. 2015, 2016; Dietrich & Ujevic 2017; Dietrich et al. 2017b,a; Bovard et al. 2017; Papenfort et al. 2018) during or shortly after the merger of the two stars, and in terms of matter that is ejected *secularly* (Siegel & Metzger 2017; Fernández et al. 2018; Fujibayashi et al. 2017), that is, on timescales  $\gtrsim 100$  ms. Of these two channels, the second component is not yet very well understood, mostly due to the lack of long-term three dimensional studies, although notable exceptions exist, starting either from simplified initial conditions (Siegel & Metzger 2017; Fernández et al. 2018) or being restricted to two spatial dimensions (Fujibayashi et al. 2017). In comparison, the dynamically ejected mass component has been explored in far greater detail, using either fully consistent microphysical descriptions at finite temperature and in full general relativity (Radice et al. 2016, 2018; Lehner et al. 2016; Sekiguchi et al. 2016; Bovard et al. 2017), or in approximations of general relativity (Bauswein et al. 2013), or using a simplified microphysics treatment (Dietrich et al. 2017b,a; Hotokezaka et al. 2013; Ciolfi et al. 2017), together with analytical expressions that try to com-

bine the abundance of data available (Dietrich & Ujevic 2017).

Another dynamically important parameter of the system influencing the ejection of mass is the spin of the individual neutron stars. Their magnitude or orientation are poorly known, although pulsar observations suggest that neutron stars in binary systems can have significant spins, such as for the binaries PSR J1807-2500B and PSR J1946+2052. Furthermore, dynamical captures in globular clusters can lead to millisecond pulsar binaries (Benacquista & Downing 2013). In practice, the extraction of information on the spin from the gravitational-wave signal of GW170817 has proved difficult so far (Zhu et al. 2018), forcing the discussion on the physical properties of GW170817 to be split between the “low-” and “high-spin” scenarios (The LIGO Scientific Collaboration & The Virgo Collaboration 2017). This uncertainty in the modelling of the dynamical mass ejection is matched by the absence of detailed studies for consistent spinning neutron-star merger simulations. Studies so far have either used inconsistent initial conditions (Kastaun et al. 2013, 2017) or a simplistic model for the description of matter (Dietrich et al. 2017a). More specifically, although Dietrich et al. (2017a) have studied in great detail the effect of spin on the gravitational-wave signal and on the mass ejection, only small dimensionless spins  $\chi \simeq 0.1$  were used. Furthermore, the absence of neutrino interactions makes it difficult to classify the reasonable amount of shock heating and composition of the ejected matter.

In this Letter we attempt to fill this gap and study the mass ejection of high spin systems up to  $\chi \simeq 0.29$  for two finite-temperature EOSs, representing both high and low compactness, with the latter being favoured by the detection (Annala et al. 2018; Most et al. 2018; Abbott et al. 2018).

## 2. METHODS

This work studies the merger and early post-merger phase of binary neutron-star coalescence with non-vanishing spins. Spinning BNS in quasi-equilibrium are modeled via the COCAL code (Tsokaros et al. 2015; Tsokaros et al. 2018), which uses three spherical grids together with a second-order finite difference scheme to invert the elliptic equations of the gravitational and fluid potentials. The formulation used to obtain the spinning configurations is a modification of the formulation of irrotational binaries where the fluid velocity is decomposed into an irrotational and a spinning part (Tichy 2011). The latter is an input quantity that controls the final dimensionless spin  $\chi$  that is quoted in this work. Here we define  $\chi := J_{\text{QL}}/(M_{\text{ADM}}/2)^2$ , where  $J_{\text{QL}}$  is the

$\chi$	$\Omega \times 10^{-3}$ [ $M_\odot^{-1}$ ]	$J_{\text{ADM}}$ [ $M_\odot^2$ ]	$P$ [ms]	$M_{\text{ej}} \times 10^{-3}$ [ $M_\odot$ ]	EOS
−0.148 (↓↓)	8.77	6.89	−3.34	4.41	TNTYST
−0.002 (00)	8.75	7.37	−258	2.73	TNTYST
0.106	8.74	7.72	4.49	0.31	TNTYST
0.287 (↑↑)	8.81	8.39	1.75	0.24	TNTYST
−0.142 (↓↓)	8.76	6.90	−4.35	1.45	BHBAΦ
−0.001 (00)	8.75	7.37	−619	0.64	BHBAΦ
0.156	8.75	7.90	3.93	0.62	BHBAΦ
0.194 (↑↑)	8.75	8.04	3.18	0.37	BHBAΦ

**Table 1.** Summary of the binaries considered. Reported are: the dimensionless spin  $\chi$ , the period  $P$ , the orbital angular frequency  $\Omega$ , the ADM angular momentum  $J_{\text{ADM}}$ , and the ejected mass  $M_{\text{ej}}$ . All binaries have  $M_{\text{ADM}} = 2.700$  and are at an initial separation of 45 km. The labels (↓↓), (00) and (↑↑) refer to reference binaries.

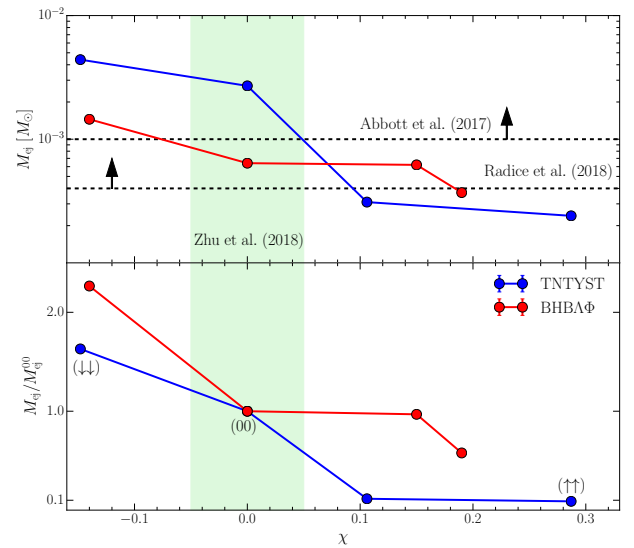


**Figure 1.** Dynamically ejected matter  $M_{\text{ej}}$  as a function of the dimensionless spin  $\chi$  of the stars in the binary. The upper panel shows the absolute value of the ejected mass, while the lower panel the relative value normalised to the irrotational case  $M_{\text{ej}}^{00}$ . The dashed lines refer to lower-bound values in the literature.

quasi-local angular momentum of each neutron star, and  $M_{\text{ADM}}$  the Arnowitt-Deser-Misner mass of the system (Tsokaros et al. 2018). In Table 1 we give an overview of the binaries studied in this work, whose components both have the same mass and a total  $M_{\text{ADM}} = 2.700 M_\odot$ . Since producing accurate initial data with high spins is computationally very demanding, we focus on only two spin configurations, either aligned (↑↑) or misaligned (↓↓) with the orbital angular momentum, but consider rotation periods of up to 1.7 ms, in line with millisecond pulsars like PSR J1748-2446ad (Hessels et al. 2006).

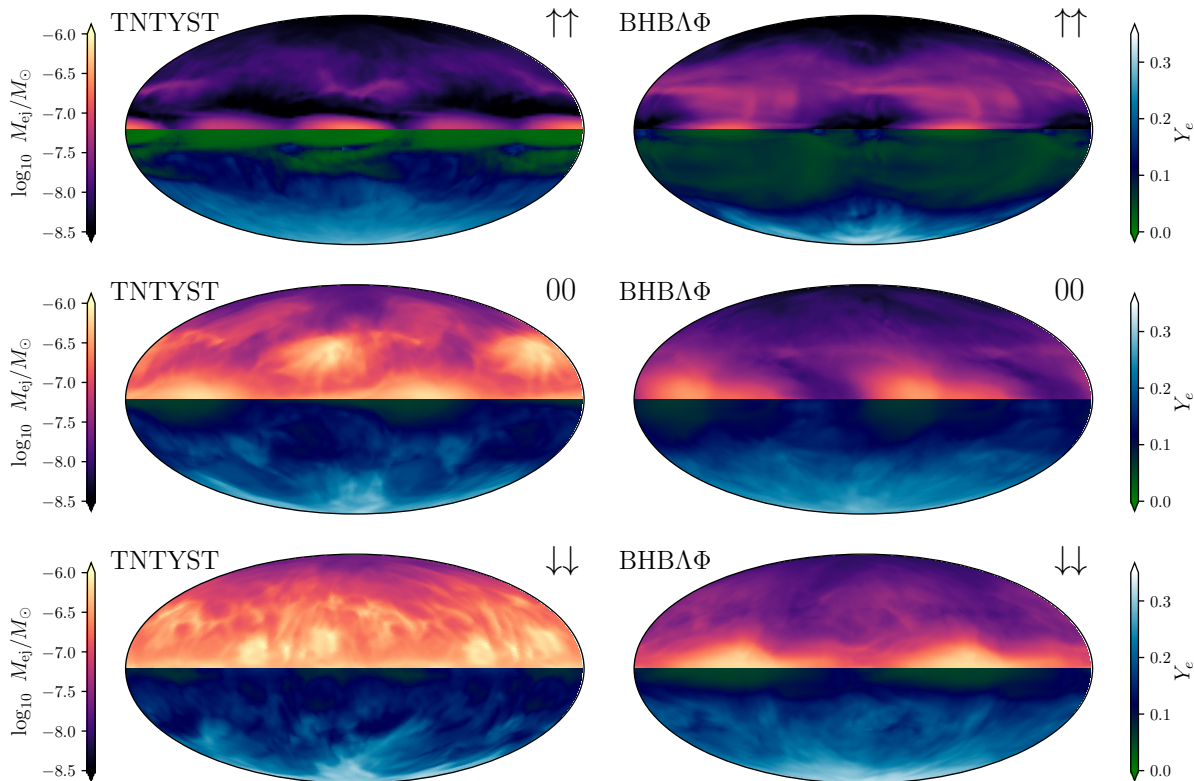


**Figure 2.** Angular distribution of the time-integrated ejected mass  $M_{\text{ej}}$  and average electron fraction  $Y_e$  for systems using the TNTYST (left column) and BHBA $\Phi$  (left column) EOS.

We solve the coupled Einstein–general-relativistic magnetohydrodynamic (GRMHD) system using the Frankfurt/IllinoisGRMHD code (FIL) (Most et al. 2019), which is derived from the IllinoisGRMHD code (Etienne et al. 2015). The GRMHD equations are solved using fourth-order accurate conservative finite differencing. To solve the Einstein equations we implement a fourth-order accurate discretization of the Z4c system (Hilditch et al. 2013). Neutrino cooling and weak interactions are incorporated via a leakage scheme Galeazzi et al. (2013). The codes makes use of the publicly available Einstein Toolkit framework (Löffler et al. 2012). The computational domain is given by a set of nested boxes in a fixed mesh refinement setting extending up to  $\simeq 1500$  km and using a total of seven levels with a highest resolution of  $\simeq 250$  m. To assess the impact of resolution, we also performed simulations for three TNTYST models at  $\simeq 370$  m and one for the irrotational system at  $\simeq 195$  m. In all cases, the relative difference were between 10% and 20%, thus much less than the uncertainty stemming from the criterion for unboundness (Bovard et al. 2017).

The final important ingredient is the description of nuclear matter at finite temperatures. In light of re-

cent studies following the detection of GW170817 (Anala et al. 2018; Most et al. 2018; Abbott et al. 2018), we select two temperature-dependent EOSs: TNTYST (Togashi et al. 2017) and BHBA $\Phi$  (Banik et al. 2014), to representing the bounds on small and high tidal deformabilities.

Every star in the binary systems is initially endowed with a poloidal magnetic field of  $10^{15}$  G at its center. While magnetic fields are very important to study secular outflows, the impact they have on the dynamical mass ejection are small (for the TNTYST irrotational binary, the magnetically induced differences in the mass ejection rates are  $\lesssim 5\%$ ) and we will not discuss them here for compactness.

### 3. RESULTS

We considered a total of eight systems modeled using two EOSs and having either spins aligned or misaligned with the orbital spin angular momentum, ignoring systems where only one of the stars is spinning (Dietrich et al. 2017a). While we plan to consider these effects in future work, we note that unequal-mass binaries are expected to yield systematically larger matter outflows (Rezzolla et al. 2010; Lehner et al. 2016; Sekiguchi et al. 2016), although for mass ratios ( $q \gtrsim 0.8$ ), this

effect is not expected to be significant (Dietrich et al. 2017a).

Depending on the spin orientation and starting from a separation of 45 km, the two stars inspiral for several orbits before they merge. As first shown by Kastaun et al. 2013, systems with large aligned spins take longer to radiate away the orbital angular momentum and will hence merge later than the systems with misaligned spin (see also Dietrich et al. 2017a; Ruiz et al. 2019, for a detailed description). After the merger, we record the mass that is unbound according to the geodesic criterion (Bovard et al. 2017) and crosses a sphere at a radius of 600 km, thus obtaining the dynamically ejected mass by an integration over roughly 15 – 20 ms, when the mass flux drops significantly in all cases. We note that all simulations were carried out for sufficiently long timescales to observe a vanishing dynamical ejection of matter and that no black hole was formed by the end of the simulations.

Before focussing on three fiducial cases – misaligned high spins ( $\downarrow\downarrow$ ), no spins (00), and aligned high spins ( $\uparrow\uparrow$ ) – we give an overview of the amount of dynamically ejected matter for all models listed in Table 1. This is shown in Fig. 1, which reports the amount of dynamically ejected mass depending on the dimensionless spin  $\chi$ . The upper panel refers to the absolute value of the ejected mass, while the lower panel emphasizes the difference with the respect to the irrotational case, which is the most common in merger simulations.

Note that intermediate misaligned spins  $\chi \sim -0.14$  lead only to a small twofold increase compared with the irrotational case, while for high aligned spins  $\chi \lesssim 0.29$  we find that large aligned spins can significantly reduce the mass ejection by about a factor of two in the case of the stiff BHBA $\Phi$  EOS and even of about one order of magnitude in the case of the soft TNTYST EOS. As a comparison, we also show in the top panel of Fig. 1 the reference bounds on the dynamical mass ejection coming either from the LIGO GW170817 analysis (Abbott et al. 2017) or by considering the models having  $M \geq 2.7 M_\odot$  in Radice et al. (2018). Clearly, most of our aligned spinning cases produce lower values than expected from these studies and this contrast in the dynamical ejecta can only become larger with unequal-mass binaries since the secondary star is tidally disrupted (Rezzolla et al. 2010). We also note that we have tried to use the fitting formulas for the dynamically ejected mass provided by Dietrich & Ujevic (2017) and calibrated by Radice et al. (2018), finding negative values when considering the TNTYST EOS. This highlights that more simulations are needed to achieve a comprehensive – and thus

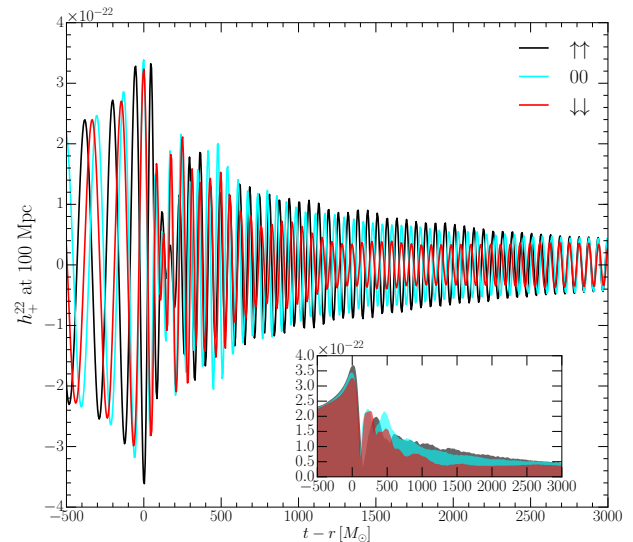


**Figure 3.** Gravitational-wave strains ( $\ell = 2 = m$  mode of the  $h_+$  polarization) for binaries with the TNTYST EOS; the amplitudes of the signals are shown in the inset.

accurate – coverage of the space of EOS and spin configurations.

To better represent the drastic change in mass ejection and also to elucidate its properties with regards to an accompanying kilonova, we show in Fig. 2 the angular distributions of the ejected mass projected onto a two-sphere at 600 km. Starting with the irrotational case (middle row in Fig. 2), the top part of the projection illustrates that ejected mass is mainly distributed along the equatorial plane as a result of tidally driven outflow (see also Sekiguchi et al. 2016; Bovard et al. 2017; Radice et al. 2018 for a more detailed discussion). The behaviour is rather similar for the two EOSs considered, but in the case of the softer TNTYST EOS, shock-heating also plays a role in the ejection of matter, which is visible at a latitude of  $\sim 45$  degrees. Additionally, the part of the same panel reports the time-averaged composition of the ejected matter, pointing out that while the tidal component is very neutron rich, i.e.,  $Y_e \lesssim 0.1$ , there are regions of high protonization at higher latitudes and conversely lower densities extending the  $Y_e$  range to  $\lesssim 0.3$ .

When contrasting the irrotational binaries with the misaligned-spin ones (bottom row in Fig. 2), it is clear that in this case most of the ejecta is driven by strong shock-heating – especially in the case of the TNTYST EOS – and are distributed to higher latitudes. This is due to the fact that the misaligned binaries not only have the smallest amount of angular momentum after merger, and so higher radial velocities in the ejecta (see also Fig. 4), but also the largest plunge velocity at



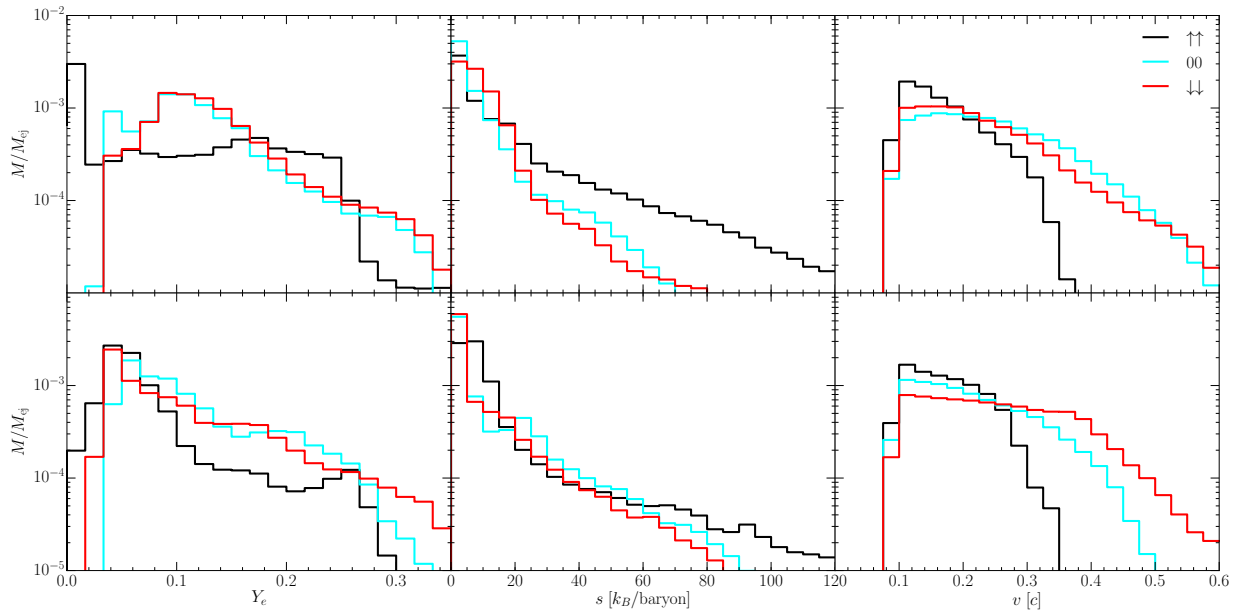


**Figure 4.** Histograms showing various composition features of the ejected mass. From left to right: the electron fraction  $Y_e$ , the entropy  $s$  per baryon and the velocity  $v$  as computed from the Lorentz factor of the outflow. The *top row* refers to models using the TNTYST EOS, while the *bottom row* to the BHBA $\Phi$  models.

merger. Indeed, these binaries inspiral with fewer orbits and merge with a radial velocity for the TNTYST (BHBA $\Phi$ ) EOS that – in units of the speed of light – is  $\simeq 0.042$  ( $0.035$ ); these plunge velocities should be compared with  $\simeq 0.028$  ( $0.027$ ) for the aligned case. On the other hand, when considering aligned high-spin binaries (top row in Fig. 2), we find that mass ejection is significantly suppressed, up to one order of magnitude for the TNTYST EOS. Furthermore, the ejection is strongly beamed towards the equator, a clear indication that the origin of the mass ejection is purely tidal, consistent with the fact of the two stars having a significantly reduced relative velocity at merger, in analogy with what happens in eccentric mergers (Radice et al. 2016; Papenfort et al. 2018). An important difference with respect to the other two cases is that the ejecta are mainly neutron rich and even the polar regions feature significantly smaller electron fractions.

Much of the phenomenology discussed above is reflected in the gravitational-wave emission from the merger remnant. Figure 3 reports the amplitude of gravitational-wave strain of the three reference cases and it is apparent that the remnant from the binary with large aligned spins is less compact because of the excess angular momentum; this more extended and “colder” object will produce comparatively larger-amplitude gravitational waves and a reduced ejection of neutron-rich matter. By contrast, the remnant from the binary with large misaligned spins is more compact

and “hotter”, with a reduced emission of gravitational waves, but a larger ejection of high- $Y_e$  matter. As expected, the irrotational binary is intermediate between these two cases.

Finally, we report in Fig. 4 the relative distributions of  $Y_e$ , of the entropy  $s$  per baryon and of the velocity  $v$  of the ejecta. For both EOSs, the behaviour is qualitatively the same: the misaligned and the irrotational binaries have similar compositions peaking around  $Y_e \simeq 0.1$  and then rapidly falling off until about  $Y_e \simeq 0.35$ . Most of these ejecta have small entropies  $s < 20 k_B/\text{baryon}$ , with  $s < 80 k_B/\text{baryon}$  almost everywhere. The material for these two systems also has outflow velocities reaching up to 0.6. On the other hand, the aligned spinning binaries have large amounts of ejecta around  $Y_e < 0.05$  and almost no material is present with  $Y_e > 0.3$ ; a cut-off in the electron fraction is present in both EOSs. Similarly, the velocity  $v$  of the ejecta in the aligned binaries peaks around small values  $v \simeq 0.1$ , pointing to the absence of strong shock heating in most of the matter, with a cut-off velocity of  $v \simeq 0.35$  for both EOSs.

#### 4. CONCLUSIONS

We have presented GRMHD simulations of neutron-star mergers having high component spins and employing two temperature-dependent EOSs representing the soft and stiff limits of current constraints (Annala et al. 2018; Most et al. 2018; Abbott et al. 2018). By varying the orientation as well as the magnitude of both stellar spins, we were able to reveal a strong impact on dy-

namical mass ejection and highlight the changes in the nuclear composition of the material. In particular, binaries with high spins aligned with the orbital angular momentum lead to a strong suppression of the ejected mass when compared to the standard case of irrotational binaries. At the same time, misaligned configurations show only a modest increase. We found that this effect was most pronounced for the soft TNTYST EOS, where it lead to a suppression of one order of magnitude compared with the non-spinning case.

The physical origin of this behaviour lies with an increased total angular momentum at merger of the binaries with aligned spins and consequently with the decreased plunge velocities when the two stars collide. In turn, this process leads to a merger remnant that is more extended and “colder” than in the case of irrotational binaries, thus with a reduced ability to shed mass dynamically, but more efficient in radiating gravitational waves. In contrast, binaries with large misaligned spins collide with larger velocities and yield, for the same EOS, a remnant that is more compact, “hotter” and less luminous in gravitational waves.

Our simulations have also shown that the spatial distribution and composition of the ejected matter vary with spin. Most notably, we have demonstrated that binaries with high aligned spins eject extremely neutron-rich material and at lower average velocities. The contrary is true for binaries with large misaligned spins. Finally, we have highlighted how neglecting the effects of high spin on the dynamical ejecta overestimates the amount of ejected mass and can in principle lead to significant deviations in the modelling of the resulting kilonova emission. This effect will be particularly important for high-mass systems that either lead to a prompt or delayed collapse within  $\lesssim 10$  ms, for which light remnant disks are be obtained (Rezzolla et al. 2010; Ruiz & Shapiro 2017) and secular mass ejection is subdominant. By measuring the peak time and magnitude of the luminosity of the red component compared to the blue component of the kilonova, which in this case will be dominated by the dynamical ejecta, it should in principle be possible to infer constraints on the spin of the system that are complementary to those obtained currently from the gravitational-wave emission during the inspiral, although modelling uncertainties in kilonova afterglow modelling still remain large. To illustrate this, we follow Abbott et al. (2017), and in the case of a soft EOS such as TNTYST, find a difference in the peak time and luminosity in kilonova emission of  $t_p^{\downarrow\downarrow}/t_p^{\uparrow\uparrow} \approx 2.2$ , and  $L_p^{\downarrow\downarrow}/L_p^{\uparrow\uparrow} \approx 4.3$ , using the values obtained from the simulations in this work.

Our simulations inevitably cover only a small but representative portion of the space of parameters. Further studies, and the development of new temperature-dependent EOSs, will be needed to set tighter constraints on how the dynamically ejected matter relates to the stiffness of the EOS and to the spin configuration. While our study only addresses equal-mass systems, the precise interplay of spin and unequal-mass systems remains to be explored. Nevertheless, the conclusions drawn in this work apply to realistic mass ratios compatible with GW170817<sup>1</sup> ( $q \gtrsim 0.8$ ), or to observed binary systems (Zhu et al. 2018),  $q \gtrsim 0.9$ . Only when extreme mass ratios are considered ( $q \lesssim 0.7$ ), spin effects could be subdominant to tidally driven mass ejection (Dietrich et al. 2017a), although the numerical error budget of these simulations remains very large. Additionally, when considering equal mass misaligned systems ( $\downarrow\downarrow$ ), we have found an increase in mass ejection similar to the one expected for moderate mass ratios  $q \gtrsim 0.9$ , highlighting a degeneracy between misaligned spinning systems and unequal-mass binaries. By incorporating finite-temperature and neutrino effects we were also able to show that the distribution of outflow is more shock heated and hence expected to be more isotropic than tidally driven mass ejection in unequal mass system. Further studies will be required to investigate whether the two effects can, hence, be discerned in observations of red and blue kilonova components, especially for high-mass systems where the secular ejection will be suppressed. Lastly, it will also be important to investigate how the difference in the angular momentum and compactness of the remnant resulting from initial spins translates to different lifetimes and disk masses after collapse to a black hole. Long-term self-consistent simulations accounting for magnetically and neutrino-driven winds will be needed to clarify this point.

## ACKNOWLEDGEMENTS

We thank Antonios Nathanail for useful discussions. Support comes in part from HGS-HIRe for FAIR; the LOEWE-Program in HIC for FAIR; “PHAROS”, COST Action CA16214 European Union’s Horizon 2020 Research and Innovation Programme (Grant 671698) (call FETHPC-1-2014, project ExaHyPE); the ERC Synergy Grant “BlackHoleCam: Imaging the Event Horizon of Black Holes” (Grant No. 610058); the National Science Foundation (NSF) Grant PHY-1662211, and NASA Grant 80NSSC17K0070. The simulations were performed on SuperMUC at LRZ in Garching, on the

<sup>1</sup> Assuming the low spin prior.

GOETHE-HLR cluster at CSC in Frankfurt, and on the HazelHen cluster at HLRS in Stuttgart.

## REFERENCES

- Abbott, B. P., Abbott, R., Abbott, T. D., et al. 2017, *Astrophys. J. Lett.*, **850**, L39
- . 2018, *Physical Review Letters*, **121**, 161101
- Annala, E., Gorda, T., Kurkela, A., & Vuorinen, A. 2018, *Phys. Rev. Lett.*, **120**, 172703
- Banik, S., Hempel, M., & Bandyopadhyay, D. 2014, *Astrophys. J. Suppl.*, **214**, 22
- Bauswein, A., Goriely, S., & Janka, H.-T. 2013, *Astrophys. J.*, **773**, 78
- Benacquista, M. J., & Downing, J. M. B. 2013, *Living Reviews in Relativity*, **16**, 4
- Bovard, L., Martin, D., Guercilena, F., et al. 2017, *Phys. Rev. D*, **96**, 124005
- Burgio, G. F., Drago, A., Pagliara, G., Schulze, H.-J., & Wei, J.-B. 2018, *Astrophys. J.*, **860**, 139
- Cioffi, R., Kastaun, W., Giacomazzo, B., et al. 2017, *Phys. Rev. D*, **95**, 063016
- Dietrich, T., Bernuzzi, S., Ujevic, M., & Tichy, W. 2017a, *Phys. Rev. D*, **95**, 044045
- Dietrich, T., & Ujevic, M. 2017, *Classical and Quantum Gravity*, **34**, 105014
- Dietrich, T., Ujevic, M., Tichy, W., Bernuzzi, S., & Brügmann, B. 2017b, *Phys. Rev. D*, **95**, 024029
- Drout, M. R., Piro, A. L., Shappee, B. J., et al. 2017, *Science*, **358**, 1570
- Etienne, Z. B., Paschalidis, V., Haas, R., Mösta, P., & Shapiro, S. L. 2015, *Class. Quantum Grav.*, **32**, 175009
- Fernández, R., Tchekhovskoy, A., Quataert, E., Foucart, F., & Kasen, D. 2018, *Mon. Not. R. Astron. Soc.*, [arXiv:1808.00461 \[astro-ph.HE\]](https://arxiv.org/abs/1808.00461)
- Fujibayashi, S., Sekiguchi, Y., Kiuchi, K., & Shibata, M. 2017, *Astrophys. J.*, **846**, 114
- Galeazzi, F., Kastaun, W., Rezzolla, L., & Font, J. A. 2013, *Phys. Rev. D*, **88**, 064009
- Hessels, J. W., Ransom, S. M., Stairs, I. H., et al. 2006, *Science*, **311**, 1901
- Hilditch, D., Bernuzzi, S., Thierfelder, M., et al. 2013, *Phys. Rev. D*, **88**, 084057
- Hotokezaka, K., Kiuchi, K., Kyutoku, K., et al. 2013, *Phys. Rev. D*, **87**, 024001
- Kasen, D., Metzger, B., Barnes, J., Quataert, E., & Ramirez-Ruiz, E. 2017, *Nature*, **551**, 80
- Kastaun, W., Cioffi, R., Endrizzi, A., & Giacomazzo, B. 2017, *Phys. Rev. D*, **96**, 043019
- Kastaun, W., Galeazzi, F., Alic, D., Rezzolla, L., & Font, J. A. 2013, *Phys. Rev. D*, **88**, 021501
- Lehner, L., Liebling, S. L., Palenzuela, C., et al. 2016, *Classical and Quantum Gravity*, **33**, 184002
- LIGO Scientific Collaboration, Virgo Collaboration, Gamma-Ray Burst Monitor, F., & INTEGRAL. 2017, *Astrophys. J. Lett.*, **848**, L13
- Löffler, F., Faber, J., Bentivegna, E., et al. 2012, *Class. Quantum Grav.*, **29**, 115001
- Margalit, B., & Metzger, B. D. 2017, *Astrophys. J. Lett.*, **850**, L19
- Most, E. R., Papenfort, L. J., Dexheimer, V., et al. 2019, *Phys. Rev. Lett.*, **122**, 061101
- Most, E. R., Weih, L. R., Rezzolla, L., & Schaffner-Bielich, J. 2018, *Phys. Rev. Lett.*, **120**, 261103
- Palenzuela, C., Liebling, S. L., Neilsen, D., et al. 2015, *Phys. Rev. D*, **92**, 044045
- Papenfort, L. J., Gold, R., & Rezzolla, L. 2018, *PhRvD*, **98**, 104028
- Radice, D., Galeazzi, F., Lippuner, J., et al. 2016, *Mon. Not. R. Astron. Soc.*, **460**, 3255
- Radice, D., Perego, A., Hotokezaka, K., et al. 2018, *Astrophys. J.*, **869**, 130
- Raithel, C., Özel, F., & Psaltis, D. 2018, *ApJ*, **857**, L23
- Rezzolla, L., Baiotti, L., Giacomazzo, B., Link, D., & Font, J. A. 2010, *Class. Quantum Grav.*, **27**, 114105
- Rezzolla, L., Most, E. R., & Weih, L. R. 2018, *Astrophys. J. Lett.*, **852**, L25
- Ruiz, M., Shapiro, S. L. 2017, *Phys. Rev. D*, **96**, 084063
- Ruiz, M., Shapiro, S. L., & Tsokaros, A. 2018, *Phys. Rev. D*, **97**, 021501
- Ruiz, M., Tsokaros, A., Paschalidis, V., & Shapiro, S. L. 2019, arXiv e-prints, [arXiv:1902.08636](https://arxiv.org/abs/1902.08636)
- Sekiguchi, Y., Kiuchi, K., Kyutoku, K., & Shibata, M. 2015, *Phys. Rev. D*, **91**, 064059
- Sekiguchi, Y., Kiuchi, K., Kyutoku, K., Shibata, M., & Taniguchi, K. 2016, *Phys. Rev. D*, **93**, 124046
- Shibata, M., Fujibayashi, S., Hotokezaka, K., et al. 2017, *Phys. Rev. D*, **96**, 123012
- Siegel, D. M., & Metzger, B. D. 2017, *Physical Review Letters*, **119**, 231102
- Tews, I., Margueron, J., & Reddy, S. 2018, *PhRvC*, **98**, 045804
- The LIGO Scientific Collaboration, & The Virgo Collaboration. 2017, *Phys. Rev. Lett.*, **119**, 161101

- Tichy, W. 2011, [Phys. Rev. D](#), **84**, 024041
- Togashi, H., Nakazato, K., Takehara, Y., et al. 2017, [Nucl. Phys.](#), **A961**, 78
- Tsokaros, A., Uryū, K., & Rezzolla, L. 2015, [Phys. Rev. D](#), **91**, 104030
- Tsokaros, A., Uryū, K., Ruiz, M., & Shapiro, S. L. 2018, [Phys. Rev.](#), **D98**, 124019
- Wollaeger, R. T., Korobkin, O., Fontes, C. J., et al. 2018, [Mon. Not. R. Astron. Soc.](#), **478**, 3298
- Zhu, X., Thrane, E., Osłowski, Stefan and Levin, Y., & Lasky, P. D. 2018, [PhRvD](#), **98**, 043002